RSC Advances

PAPER

View Article Online
View Journal | View Issue

Cite this: *RSC Adv.*, 2017, **7**, 39748

Li states on a C–H vacancy in *graphane*: a first-principles study

R. E. Mapasha, *[a] M. P. Molepo[b] and N. Chetty[ac]

Using a hybrid density functional theory approach, we have studied the effect of the interaction of a Li atom with a C–H pair vacancy defect (V_{CH}) in a *graphane* monolayer on the thermodynamic stability, structural, magnetic and electronic properties, taking into account the effect of charge doping. We found that a Li atom and charge doping enhanced the thermodynamic stability of a V_{CH} defective *graphane* monolayer. The Li–V_{CH} system may likely act as a single deep donor, and can readily compensate the acceptor. The effects of Li introduce more occupied states in the band gap, and there exists strong hybridization between the C 2p states and Li 2s states at the vicinity of the Fermi level (E_F) responsible for the large magnetic moment noted. The −1 charge doping (Li^{1-}–V_{CH}) further populates the occupied states in the band gap, shifting the E_F towards the conduction band minimum. Consequently, the Li^{1-}–V_{CH} system possesses spintronic effects such as half-metallic ferromagnetic character and pronounced magnetism. The +1 charge doping (Li^{1+}–V_{CH}) removes some of the Li induced occupied states, slightly shifting the E_F towards the valence band maximum leading to a reduction in the magnetic moment. Our findings give an explanation of the origin of magnetism in a V_{CH} defective *graphane* system and suggest a possible practical way of controlling it.

Received 8th June 2017
Accepted 2nd August 2017

DOI: 10.1039/c7ra06431d

rsc.li/rsc-advances

Introduction

Graphane,[1–3] a fully hydrogenated graphene monolayer,[4–8] continues to gain research attention because of its special properties such as high volumetric hydrogen density and a wide direct energy band gap.[9–14] Elias *et al.*[2] reported that *graphane* samples are thermodynamically stable at room temperature. Collectively, this is evidence that a *graphane* system can be an excellent candidate for energy storage devices and room temperature nano-technological devices.

Just like in many real materials, Elias *et al.*[2] reported that *graphane* samples contain defects. The hydrogen (H) vacancies (V_H) in a *graphane* monolayer are simple defects that one can consider and are the most frequently studied.[14–22] Although defects can improve or deteriorate the quality of a material, several density functional theory (DFT) studies[14,21,22] have consistently shown that a V_H defect introduces magnetism in a *graphane* monolayer and provides a localized magnetic moment of 1 μ_B per vacancy. Experimental characterizations revealed the magnetic features in a near fully hydrogenated graphene.[23] It was suggested that this magnetism originates from the missing H, when it leaves an unpaired electron in the lone dangling bond connecting the C atom.[19] Very recently, Mapasha *et al.*[22] have investigated the effect of charge doping on the electronic properties of the V_H vacancy in a *graphane* monolayer using the DFT method. It was found that charge doping fine tunes the electronic structure of this defective system. Other previous studies reported that the magnetic moment of the V_H vacancy can be increased (suppressed) by adsorption of transition metals[19] (radicals[21]). Generally, it was concluded that a V_H defect can be used to design spintronic devices.

The other experimentally reported defects in *graphane* samples are carbon (C) vacancies.[2] It was reported that this type of defect occurs unintentionally during the process of hydrogenating graphene. Since every C is bonded to a H atom in the *graphane* model, when modeling a C vacancy, both atoms have to be removed as a C–H pair (V_{CH}). The intentional creation of a V_{CH} defect can be achieved experimentally using a high-energy ion beam. It was reported that synthesis of a V_{CH} defect should be much easier than that of V_H.[18] It has been established that the structural reorganization induced by a V_{CH} defect in a *graphane* monolayer is qualitatively different from that seen in graphene with a C vacancy as emphasized by Pujari *et al.*[24] In the case of graphene, two of the C atoms around the defect reorganize to form a σ bond stabilizing in a pentagon-like defect structure.[25,26] On the contrary, there is no σ bond formation amongst the three C atoms surrounding a V_{CH} defect in a *graphane* monolayer.[24] It is of interest to consider charge

[a]*Department of Physics, University of Pretoria, Pretoria 0002, South Africa. E-mail: edwin.mapasha@up.ac.za*

[b]*College of Graduate Studies, University of South Africa, UNISA, 0003 Pretoria, South Africa*

[c]*National Institute for Theoretical Physics, Johannesburg, 2000, South Africa*

doping and foreign atom adsorption as possibilities for stabilizing the V_{CH} defect structure.

DFT studies further reported that a V_{CH} defect induces the mid gap states with a permanent magnetic moment of 1 μ_B in a *graphane* monolayer.[18,24] These magnetic features were experimentally detected by Elias *et al.*[2] during the synthesis of *graphane* samples. The obtained magnetic moment arises from the dangling bonds on the three C atoms surrounding the V_{CH} vacancy, mainly contributed by the C 2p orbital electronic configuration. To prove this, the C dangling bonds were saturated using H atoms, and the resulting structure stabilized into a non-magnetic character.[18,24] Lithium (Li), belonging to the same periodic table group as H, is well known for its H opposing trend when doped on the graphene system.[27–32] Inspired by this, it is worth investigating how the interaction of C dangling bonds surrounding a V_{CH} vacancy with a Li atom would affect the induced magnetism as well as the thermodynamic stability. This could be a way of controlling the induced magnetism in a V_{CH} defected *graphane* which could be essential for technological devices. Although there is no literature on the Li adatom above the V_{CH} vacancy, a few studies of Li on pristine *graphane* are available.[33–37] It has been reported that the single Li adatom prefers to bind with the substrate as opposed to the Li clusters, at zero kelvin.[33–36] The Li adatom introduces mid-gap states within the *graphane* band gap.[34–36] The latter was confirmed experimentally using angle resolved photoelectron microscopy.[37] It is worthwhile in this study to investigate how the Li adatom binds with the V_{CH} vacancy, and the hybridization between the Li 2s and dangling C 2p orbitals within the band gap.

In semiconductors, defects can exist in multiple charge states due to variation in the electronic chemical potential (Fermi level) from the valence band maximum (VBM) to conduction band minimum (CBM) with respect to the change in the charge doping (addition of electrons or holes).[38] Experimentally, the variation in Fermi level occurs by applying an electric field. Through charge state modulation, the defect local structure can be altered and result in the new thermodynamic ground state of the system. Knowledge of the stable charge states of the defect and the Fermi level position where the new charge takes over (thermodynamic transition level), in terms of stability within the band gap of the semiconductor, is essential for nanotechnology device operation. The charge states in the band gap of a semiconductor are usually observed using *ab initio* methods and experimental techniques such as deep level transient spectroscopy (DLTS) and electron paramagnetic resonance (EPR) when identifying the thermodynamic transition levels.[38] It is worthwhile in this study to investigate the local structure and the thermodynamic stability of the V_{CH} vacancy defect without and with Li with different charge states, since this knowledge is still scarce.

It is essential to examine how charge modulation controls the defect induced magnetism, which is the basic requirement for nano-scale spintronic application devices. It is well known that the standard DFT functionals severely underestimate the band gaps of semiconductors, which can easily lead to wrong predictions for transition levels and defect states positions. To avoid this, we use the screened hybrid exchange correlation functional developed by Heyd, Scuseria, and Ernzerhof (HSE06 functional)[39,40] that has been proven to accurately predict the correct value of the band gap and defect transition levels in doped semiconductors.[41,42]

In this paper, we use hybrid DFT to study the thermodynamic stability and structural and magnetic properties of a V_{CH} vacancy considering the effect of charge doping. Furthermore, the interaction of a Li atom with a V_{CH} vacancy is investigated, also considering the effect of charge states. Generally, we report that the defect induced properties in a *graphane* monolayer critically depend on the charge states. This study provides a way of inducing, increasing and controlling magnetism in a *graphane* monolayer by creating defects and modulating their charge states, which is a basic requirement for designing nanoelectronic devices.

Computational details

Our electronic structure calculations were performed using the DFT approach implemented within the Vienna *ab initio* simulation packages (VASP) code.[43–46] For the description of the exchange–correlation interaction, the Heyd, Scuseria, and Ernzerhof functional (HSE06 functional)[39,40] was employed. For the core electron and chemically active valence electron interactions, the projector augmented wave (PAW) method[47] was used for the generation of the pseudopotentials. For the plane wave functions expansion, an energy cut-off of 500 eV was set. For the integration of the hexagonal Brillouin zone of a 1×1 unit cell, the $10 \times 10 \times 1$ *k*-mesh generated using the Monkhorst–Pack scheme[48] is sufficient to yield accurate results. However, for the large supercell system, a $4 \times 4 \times 1$ *k*-mesh is suitable for the integration. We employed the Methfessel–Paxton (MP) scheme[49] to populate the electronic states in the self-consistent field calculations. Our supercell structures were allowed to relax until the residual atomic forces were reduced to less than 0.01 eV $Å^{-1}$, using the Hellman–Feynman theorem. During the self-consistent field calculations, the total energy was allowed to converge to within 10^{-7} eV. The supercell periodic boundary conditions are considered in this study and the interlayer spacing along the *z*-axis was set to 15 Å to significantly reduce the periodic image interactions.

To gain an insight into the stability of a V_{CH} defect at different charge states *q* within the *graphane* band gap, the formation energy should be evaluated using the following expression,

$$E_f^q(V_{CH}) = E_{tot}^q(V_{CH}) - E_{tot}(G) - \sum_i n_i\mu_i + q(E_F + \varepsilon_v) + E_{corr}^{MP}. \quad (1)$$

The term $E_{tot}^q(V_{CH})$ is the total energy of a *graphane* supercell with a V_{CH} defect in a charge state *q*, and $E_{tot}(G)$ is the total energy of the equivalent pristine *graphane* supercell. The parameter n_i is the number of atoms *i* (C and H) removed from a *graphane* supercell. μ_i refers to the chemical potentials of the reservoir of the removed H and C atoms. The chemical potential

of the H atom is obtained from the converged total energy of an isolated H_2 molecule placed in a cubic cell of lattice constants $a = b = c = 15$ Å, whereas that of C is from a fully relaxed graphene monolayer supercell.

The Fermi level E_F is an electronic chemical potential of the electron reservoir. The ε_v variable is usually the energy level valence band maximum (VBM) of a pristine *graphane* system. To significantly reduce the effects of spurious electrostatic interactions of the periodic images introduced by charge doping on the defects, the Markov–Payne[50] correction potential term E_{corr}^{MP} was included in eqn (1). The detailed description of the E_{corr}^{MP} term is found in ref. 50. This term should not be ignored to avoid the introduction of errors into the total energy of the system that might affect the accuracy of the formation energy values, although its contribution is very small in this study. To calculate the formation energy of the Li on V_{CH} vacancy defect (Li–V_{CH}) at each nominal charge state q, eqn (1) is modified as follows,

$$E_f^q(\mathrm{Li} - V_{CH}) = E_{tot}^q(V_{CH} - \mathrm{Li}) - E_{tot}(\mathrm{G}) - \sum_i n_i\mu_i + q(E_F + \varepsilon_v) + E_{corr}^{MP}, \quad (2)$$

where $E_{tot}(V_{CH}\text{–Li})$ is the total energy of the Li–V_{CH} configuration in a 7×7 *graphane* supercell. The chemical potential of the Li atom is obtained from the body centered cube (BCC) structure. To calculate the possible thermodynamic transition energy levels $\varepsilon(q/q')$ of a V_{CH} defect, the following expression is appropriate:

$$\varepsilon\left(q/q'\right) = \frac{E_f(V_{CH}^q) - E_f\left(V_{CH}^{q'}\right)}{q' - q}, \quad (3)$$

where $E_f(V_{CH}^q)$ and $E_f(V_{CH}^{q'})$ are the formation energies of the V_{CH} configuration in the charge states q and q' respectively, when the position of the E_F is pinned at the VBM. To calculate $\varepsilon(q/q')$ for the Li–V_{CH} defect configuration, eqn (3) is modified to

$$\varepsilon\left(q/q'\right) = \frac{E_f(V_{CH} - \mathrm{Li}^q) - E_f\left(V_{CH} - \mathrm{Li}^{q'}\right)}{q' - q}, \quad (4)$$

where $E_f(V_{CH}\text{–Li}^q)$ and $E_f(V_{CH}\text{–Li}^{q'})$ are the formation energies of the Li–V_{CH} configuration in the charge states q and q' obtained using eqn (2).

Results and discussion

Pristine *graphane* properties

It is important to first report the structural and electronic properties of a pristine *graphane* monolayer obtained using both the generalized gradient approximation of Perdew, Burke and Ernzerhof (GGA-PBE)[51] and hybrid HSE06 functionals. The purpose of this section is to prove that HSE06 functionals can accurately predict the band gap of a pristine *graphane* system. A previous study demonstrated that *graphane* can be modeled in different configurations or isomers such as chair-like, boat-like and armchair-like.[1] The review article of Sahin *et al.*[14] and references therein summarize other possible *graphane* isomers. The chair-like configuration was reported to be the most energetically stable as compared to other isomers,[1,14] and was also experimentally synthesized.[2] Based on this information, all our calculations were performed employing a chair-like model structure.

Fig. 1(a) presents a fully optimized chair-like *graphane* model structure. We report that although both the GGA-PBE and HSE06 functionals give the same structural appearance of *graphane*, they differ slightly in predicting the structural parameters, as shown in Table 1. The HSE06 and GGA-PBE functionals predict the lattice constant as 2.51 Å and 2.54 Å respectively. These values are in excellent agreement with the previous results shown in Table 1. Comparing the two functionals, it is noted that the HSE06 lattice constant is approximately 1% lower than the GGA-PBE value. The HSE06 and GGA-PBE functionals predict the C–C bond length d(C–C) as 1.52 Å and 1.54 Å respectively. This d(C–C) value is in good agreement with the previous theoretical data presented in Table 1. Generally, the inclusion of some portion of exact Hartree–Fock (HF) exchange in a DFT expression slightly shortens the bond distances in the carbon material systems.[40]

The spin polarized TDOS plot for a pristine *graphane* monolayer calculated using both the GGA-PBE and HSE06 functionals is shown in Fig. 1(b). In agreement with the previous study,[12] the shape of the HSE06 TDOS is almost identical to that of GGA-PBE for the entire plot, except that the TDOS for HSE06 shows a relatively larger energy band gap. Both functionals predict that a pristine *graphane* monolayer is a wide band gap semiconductor, where the quantities are shown in Table 1. Based on experimental measurements, Elias *et al.*[2] revealed that *graphane* possesses insulating features, without reporting the magnitude of the band gap. The GGA-PBE functional predicts a band gap of 3.38 eV. Since it is well known that a GGA-PBE functional is inadequate (underestimates) in predicting the band gaps of semiconductors, the use of the HSE06 functional is able to reduce the underestimation by predicting a value of 4.39 eV. This value is in good agreement with the HSE06 values reported in previous studies.[12,52,53] Based on this, we employed the HSE06 functional in the subsequent calculations of a V_{CH} vacancy in a *graphane* monolayer.

Properties of a V_{CH} defect in a graphane monolayer

As mentioned earlier, when modeling a C vacancy in *graphane*, both the C and H atoms have to be removed as a pair (V_{CH}) since every C is bonded to a H atom as shown in Fig. 2(a). This type of defect in a *graphane* monolayer sample is easily realizable experimentally and can be stable at room temperature for a long time without any characteristic alteration.[2] In this section, we studied the thermodynamic stability, structural, electronic and magnetic properties of a V_{CH} defect in a *graphane* monolayer system. The effects of different V_{CH} defect charge states $q = -2$, -1, 0, +1, and +2, and the variation in Fermi level (E_F) position within the band gap were considered.

For the thermodynamic stability analysis, the formation energy $E_f^q(V_{CH})$ of a V_{CH} vacancy at each charge state was calculated using eqn (1). Firstly, the total energy of a V_{CH} vacancy was converged as a function of the supercell sizes of $3 \times$

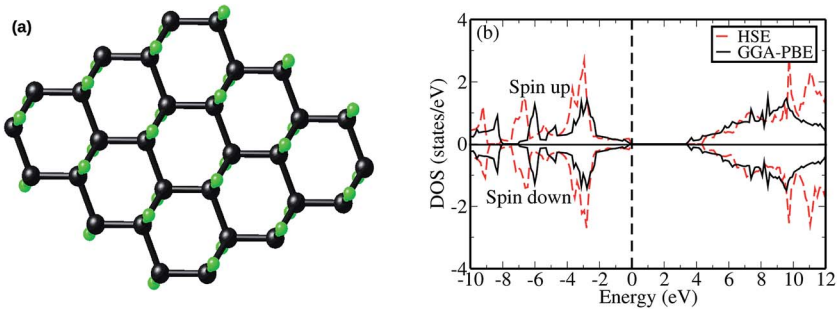

Fig. 1 (a) A relaxed geometry of a *graphane* monolayer. The carbon and hydrogen atoms are represented by black and light green spheres respectively, on a *graphane* model diagram. (b) The total density of states (TDOS) for a chair-like *graphane* model calculated using the GGA-PBE (black solid line) and HSE06 (red dashed line) functionals. The Fermi level is set at zero energy (indicated by the black dashed vertical line).

Table 1 The calculated equilibrium lattice constant *a* (in Å), distance between two nearest neighbour carbon atoms *d*(C–C) (in Å) and energy band gap E_{gap} (in eV)

	Functionals	*a*	*d*(C–C)	E_{gap}
This work	HSE06	2.51	1.52	4.39
	PBE	2.54	1.54	3.38
Other work	HSE06	2.52[a]	1.53[a]	4.60[a]
	HSE06	—	—	4.49[b]
	HSE06	2.52[c]	1.53[c]	4.38[c]
	PBE	2.54[a,c,d]	1.54[a,c,d]	3.60[a]
	PBE	2.52[e]	1.52[e]	3.50[c,d,e,f,g]

[a] Ref. 12. [b] Ref. 52. [c] Ref. 53. [d] Ref. 9. [e] Ref. 1. [f] Ref. 54. [g] Ref. 15.

3, 5 × 5, 7 × 7 and 9 × 9. For each supercell size, the formation energy $E_f^q(V_{CH})$ at $q = 0$ was calculated using eqn (1). The $E_f^q(V_{CH})$ values of 5.83 eV, 5.99 eV, 6.02 eV and 6.05 eV, corresponding respectively to 3 × 3, 5 × 5, 7 × 7 and 9 × 9 sizes, were obtained. Although it is clearly noted that convergence starts at 5 × 5, the 7 × 7 supercell has been used for the subsequent calculations. The formation energies $E_f^q(V_{CH})$ of a V_{CH} vacancy in the multiple charge states 0 (V_{CH}^0), −1 (V_{CH}^{1-}), −2 (V_{CH}^{2-}), +1 (V_{CH}^{1+}) and +2 (V_{CH}^{2+}) as a function of E_F are shown in Fig. 2(b). The values of $E_f^q(V_{CH})$ are allowed to vary within the energy band gap (ranging from 0 eV to 4.39 eV).

The $E_f^q(V_{CH})$ of the V_{CH}^{1+} and V_{CH}^{2+} systems decrease when the position of E_F approaches the VBM, while those of the V_{CH}^{1-} and V_{CH}^{2-} systems decrease when E_F shifts up towards the CBM as shown in Fig. 2(b). This indicates that a V_{CH} defect would be likely to act as a source of both acceptor and donor compensation depending on the position of E_F. Fig. 2(b) shows that the V_{CH}^{1+} vacancy system has the lowest formation energy from the VBM ($E_F = 0$ eV) to $E_F = 2.13$ eV, followed by the V_{CH}^0 system from $E_F = 2.13$ eV to 3.35 eV, and at the far end of the band gap, the V_{CH}^{1-} system is most stable from $E_F = 3.35$ eV to the CBM. Since it is noted that only the −1, 0 and +1 charge states are thermodynamically stable within the *graphane* band gap, the −2 and +2 charge states were excluded in the subsequent calculations. We further calculated the V_{CH} vacancy thermodynamic transition levels $\varepsilon(q/q')$ using eqn (3). The obtained $\varepsilon(q/q')$ values are indicated by the intersection of the two formation energy lines of the charge states q and q' shown in Fig. 2(b). Our calculations predict the donor (0/+1) and acceptor (−1/0) levels occurring at $E_v = +2.13$ eV and $E_c = -1.04$ eV respectively. The position of the donor (0/+1) level reveals that a V_{CH} defect may likely act as a deep donor. More likely, these results suggest that a V_{CH} defect will be too deep to be ionized. If the DLTS spectrum of a V_{CH} defect can be recorded, we suggest that the two peaks corresponding to the (0/+1) and (−1/0) deep levels should be observable at higher temperatures. Since it has been reported that the HSE06 functional is able to correctly mimic

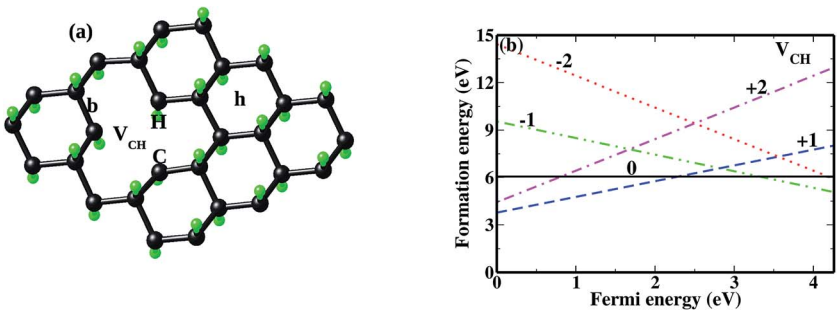

Fig. 2 (a) The local structure of a C–H vacancy (V_{CH}) in a *graphane* monolayer. (b) The V_{CH} formation energy as a function of E_F for the 0 (V_{CH}^0), −1 (V_{CH}^{1-}), −2 (V_{CH}^{2-}), +1 (V_{CH}^{1+}) and +2 (V_{CH}^{2+}) charge states. The points where the two lines intersect coincide with the thermodynamic transition levels.

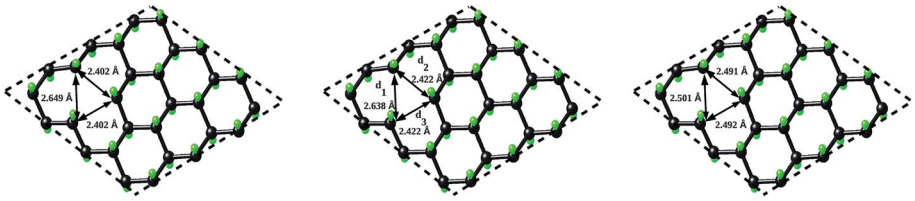

(a) V_{CH}^{-1} (b) V_{CH}^{0} (c) V_{CH}^{+1}

Fig. 3 The optimized local structure of a V_{CH} defect in a *graphane* monolayer calculated in the −1 (a), 0 (b) and +1 (c) charge states. The distances d_1, d_2 and d_3 are C–C dangling bond lengths surrounding the V_{CH} defect.

experiments in identifying the transition levels in semiconductors,[41,42] we expect our calculated values to agree very well with future experimental results.

We further examined the dependence of local geometry of a V_{CH} defect on the −1, 0 and +1 charge states. The atomic relaxation of the V_{CH} defect in the multiple charge states is shown in Fig. 3(a) for −1, Fig. 3(b) for 0 and Fig. 3(c) for +1. During relaxation, the three C atoms surrounding the V_{CH} vacancy undergo significant structural distortions, and thus the *graphane* monolayer threefold symmetry breaks due to the Jahn–Teller effect. These three C atoms surrounding the V_{CH} defect form an asymmetric triangle-like arrangement (shape), as shown in Fig. 3.

In the 0 charge state (V_{CH}^{0}), the three C atoms are slightly displaced away from the V_{CH} vacancy defect after relaxation. As

Table 2 The calculated binding energy E_b (eV) and Li equilibrium adatom height Δh (Å) above the adsorption site. The positive E_b indicates that the structure is energetically stable. To quantify the interaction between Li and the *graphane* system, the amount of charge transfer q was calculated using the Bader charge analysis.[57] These properties were obtained after the atomic position relaxation calculations

Adsorption site	E_b (eV)	q (e)	Δh (Å)
Li–V_{CH}	1.72	0.87	1.54
Li–C	0.60	0.82	1.66
Li-h	0.58	0.96	1.70
Li–H	−1.19	0.19	4.19
Li-b	0.96	0.80	1.59

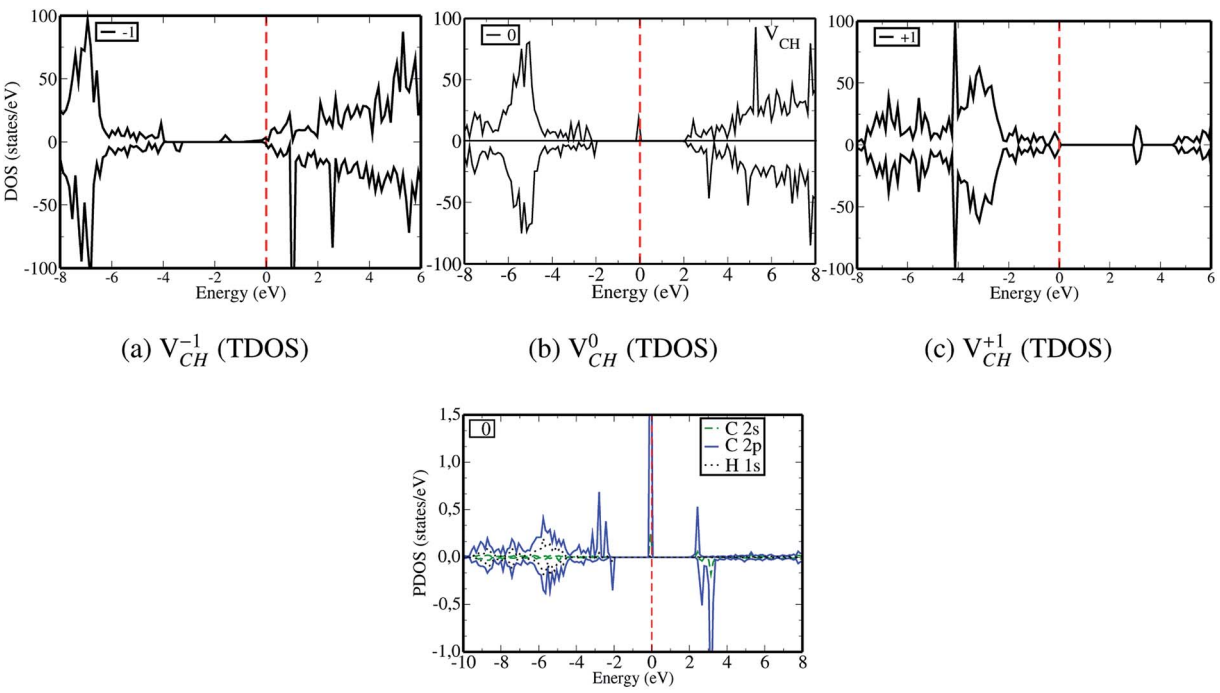

(a) V_{CH}^{-1} (TDOS) (b) V_{CH}^{0} (TDOS) (c) V_{CH}^{+1} (TDOS)

(d) V_{CH}^{0} (PDOS)

Fig. 4 The spin polarized total density of states (TDOS) for V_{CH} calculated in the −1 (a), 0 (b) and +1 (c) charge states. The partial density of states (PDOS) for a V_{CH} defect calculated in the 0 charge state (d). The Fermi level at 0 eV is shown by the dashed vertical line.

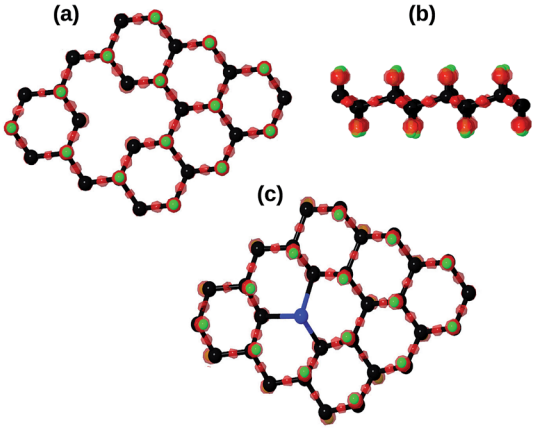

Fig. 5 Iso-surfaces of difference charge density distribution. (a) Top view of difference charge density distribution on the V_{CH} vacancy in a *graphane* monolayer. (b) Side view of V_{CH} vacancy is shown to clearly indicate that no charge is accumulated on the C atom but on the H atom. (c) Top view of difference charge density distribution after the adsorption of the Li atom on the V_{CH} vacancy (Li–V_{CH}) in the *graphane* monolayer. The blue, green and black atoms represent the Li, H and C atoms respectively. For comparison purposes, these plots were generated at the same iso-surface value scale.

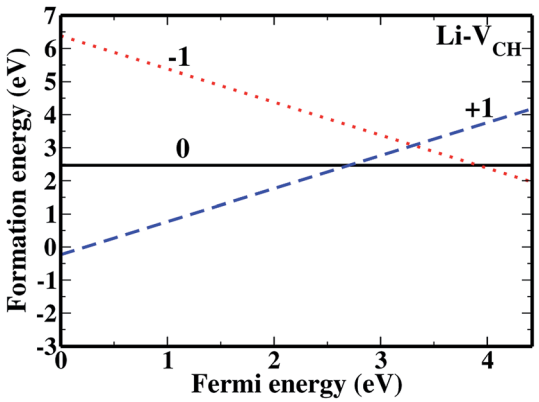

Fig. 6 The formation energies for Li^{1-}–V_{CH}, Li^{0}–V_{CH} and Li^{1+}–V_{CH} as a function of E_F. The points where the two lines intersect coincide with the thermodynamic transition levels.

a result, our relaxed C–C dangling bond distances d_1, d_2 and d_3 constructing a triangle-like shape are 2.64 Å, 2.42 Å and 2.42 Å respectively. Our calculated HSE06 values are about 0.10 Å less than the GGA-PBE values reported by Pujari *et al.*,[24] although the trend is the same. The slightly shorter bond distances in our calculations should be attributed to the use of exact short range Hartree–Fock (HF) exchange, that usually underestimates the structure of carbon systems with a very small magnitude.[40]

Since creation of a V_{CH} defect in a *graphane* model structure leaves the three nearest neighbour (adjacent) C atoms surrounding the vacancy, each with a dangling bond, we suggest that the bond distance d_1 separates the two carbon atoms of the same electronic spin, whereas d_2 and d_3 separate those of opposite spins. Thus, the relatively large value of d_1 should be attributed to a high Coulomb repulsion of the same spin electrons, as compared to those of the opposite spins (d_2 and d_3). In order to understand the effect of a V_{CH} defect on the electronic structure of a *graphane* monolayer, the TDOS were evaluated and presented in Fig. 4. Fig. 4(b) shows the TDOS for a V^0_{CH} defect. The V^0_{CH} defect induces the spin polarized mid gap states with a sharp peak crossing the E_F. Experimental characterization of *graphane* revealed that the deep defect levels are due to the absence of H[23] or C[2] occurring during the synthesis. Moreover, these partially occupied mid gap states appear only in the spin-up channel at the E_F, revealing a half-metallic character. This spintronic effect is crucial in the developing nanoelectronic field. The fascinating half-metallic nature in a V^0_{CH} defect system might be attributed to the effect of dangling bonds from the three carbon atoms surrounding the V_{CH} defect. In agreement with previous studies,[24] this system is ferromagnetic with an integral magnetic moment of 1.0 μ_B.

The obtained magnetic moment of 1.0 μ_B in the three dangling bonds system can be explained as follows; since it is well known that each dangling bond should contribute to 1.0 μ_B, the dangling bonds on the two C atoms of different electronic spins pair, and thus result in cancellation of their magnetic moment contributions. Consequently, the resulting magnetic moment of 1.0 μ_B in a V^0_{CH} defected *graphane* mainly arises from the third C atom that has an unpaired electron. To examine the stability of the induced magnetic state, the magnetization energy as the total energy difference between the spin imposed TDOS (spin-polarized) and that of the non-spin imposed TDOS (non-spin polarized) was calculated. Our calculated magnetization energy is −169 meV. The negative sign shows that a V^0_{CH} defect is more energetically stable in a spin-polarized state than in a non-spin polarized state, revealing that the ground state of this defective system is magnetic. Our calculated magnetization energy is more than the room temperature thermal energy of 25 meV, indicating that theV^0_{CH} defect-induced magnetism is relatively too strong. We further calculated the partial density of states (PDOS) for a V^0_{CH} defect system to explore the origin of its magnetism. Fig. 4(d) shows the PDOS for one polarized C atom adjacent to the V_{CH}. The pronounced peak states seen crossing the E_F in Fig. 4(d) originate from the C 2p orbital electronic configuration in agreement with Pujari *et al.*[24] The C 2s orbital has a small contribution of about 0.2 states per eV. This reveals that the noted magnetic moment in a V^0_{CH} defect predominantly originates from the polarized C 2p orbital, with little contribution from the C 2s orbital. The H atom attached to this polarized C atom site does not have any magnetic influence.

Fig. 3(a) clearly indicates that the bond distances surrounding a V_{CH} defect are sensitive to charge doping. The effect of −1 charge doping (V^{1-}_{CH}) is to expand the distance d_1 by the magnitude of 0.02 Å and reduce d_2 and d_3 by 0.01 Å relative to the values for V^0_{CH}. This indicates that an addition of an electron into this system slightly increases the coulomb repulsion between the two C atoms suggested to have electrons of the same spin. Fig. 4(a) shows that charge doping into a V_{CH} defect does not only affect the geometrical structure but also the electronic properties. An addition of −1 charge state still gives the ground state spin polarized TDOS, but doubles the total

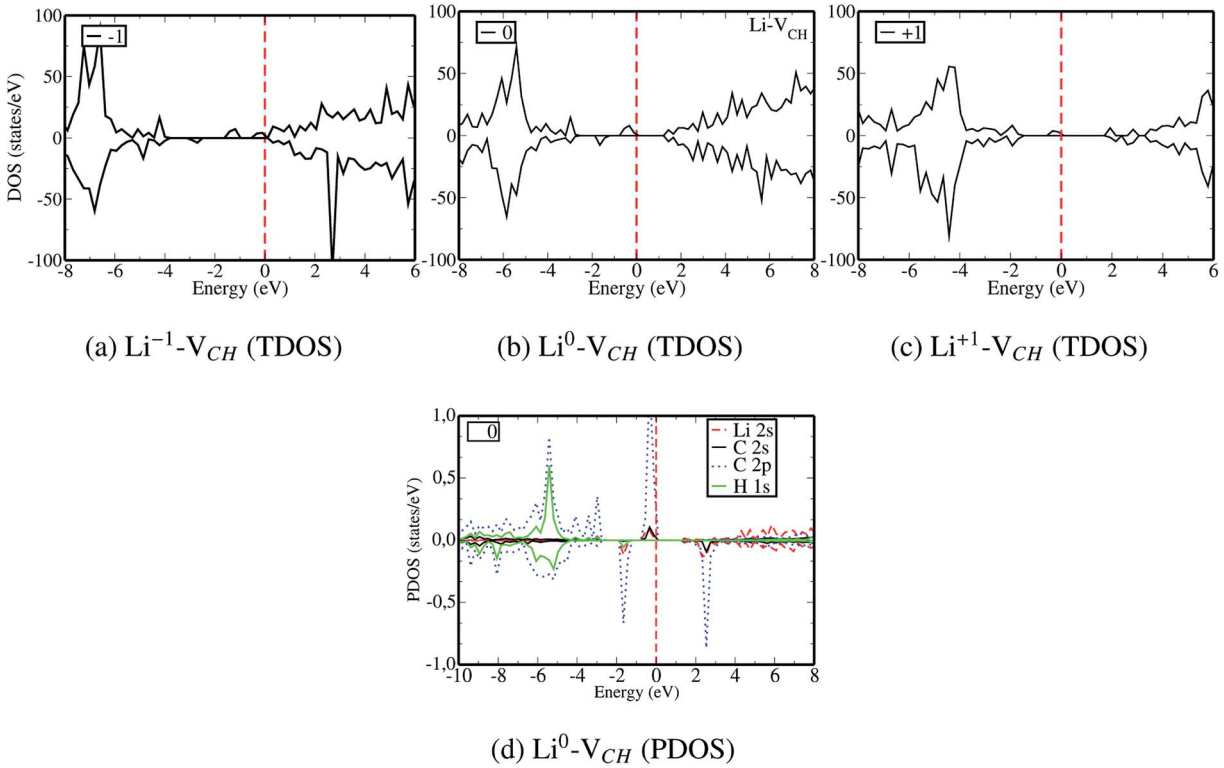

Fig. 7 The spin polarized total density of states (TDOS) for Li–V_{CH} in a *graphane* monolayer computed in different charge states: (a) Li^{1-}–V_{CH}, (b) Li^{0}–V_{CH} and (c) Li^{1+}–V_{CH}. (d) The partial density of states (PDOS) for Li^{0}–V_{CH}. The Fermi level (at $E_F = 0$ eV) is represented by the dashed vertical line.

magnetic moment (2.0 μ_B). We also note that the effect of −1 charge doping introduces extra occupied spin-down states within the band gap and also pushes the E_F to the CBM position, revealing that a V_{CH}^{1-} defect is a typical n-type defect. This E_F shift completely destroys the half-metallic character (see Fig. 4(a)).

A different scenario is noted when the +1 charge is doped into the system V_{CH}^{1+}. The distance d_1 decreases significantly by the magnitude of 0.14 Å, while d_2 and d_3 expand by 0.07 Å relative to the values of V_{CH}^{0}. It is clear that an addition of +1 charge enforces structural reconstruction around the V_{CH} defect, because d_1 is almost equal to d_2 and d_3. This further suggests that the relaxation of a V_{CH}^{1+} defect is trying to preserve the hexagonal 3-fold symmetry. From the TDOS plot of V_{CH}^{1+} shown in Fig. 4(c), it is noted that the spin-up TDOS and spin-down TDOS are invertibly symmetrical, revealing that the ground state of a V_{CH}^{1+} defect is non-spin polarized and has no magnetic moment. As mentioned earlier, creation of a V_{CH} defect leaves its three neighboring C atoms having an unpaired excited electron each. Then, withdrawal of an electron by the addition of a +1 charge leaves two excited electrons. The non-spin polarization ground state in the V_{CH}^{1+} defect confirms that the two polarized electrons pair after structural relaxation. Fig. 4(c) also shows that the E_F has been shifted to the top of the VBM, indicating that a V_{CH}^{1+} defect has a deficiency of electrons. In conclusion, the electronic structure of a V_{CH} defect in the *graphane* monolayer can be altered *via* charge state modulation.

Properties of Li adatom above the V_{CH} vacancy in a *graphane* monolayer

We further investigated the effects of Li on the induced electronic states localized on the three adjacent C atoms surrounding the V_{CH} defect site, on the same level of accuracy. Firstly, the Li adatom preferred site on a *graphane* structure was examined from the binding energies (E_b) calculation analysis. Fig. 2(a) presents the possible Li adsorption sites surrounding the V_{CH} defect in a *graphane* geometry model. The following sites were considered; (1) Li adatom above the center of a hexagon (Li-h), (2) Li adatom above the V_{CH} defect (Li–V_{CH}), (3) Li adatom above the hydrogen atom (Li–H), (4) Li adatom above the carbon atom (Li–C) that is bonded to a H atom on the other side of the layer and (5) Li adatom above the midpoint between the two nearest neighbour carbon atoms also known as a bridge site (Li-b). To find the most energetically favourable site, the binding energy of each Li configuration was calculated using the following expression;

$$E_b = E_{tot}(V_{CH} + Li) - E_{tot}(V_{CH}) - E_{tot}(Li), \quad (5)$$

where $E_{tot}(V_{CH} + Li)$ and $E_{tot}(V_{CH})$ terms are the total energies of a V_{CH} vacancy in a *graphane* monolayer with and without a Li adatom respectively. The term $E_{tot}(Li)$ is the converged energy of an isolated Li adatom. Table 2 presents the obtained binding energies of all the Li configurations considered. We also

calculated the Li equilibrium height (Δh) of all the considered configurations, also summarized in Table 2.

Table 2 shows that the Li–V_{CH} configuration is the preferred site with the highest binding energy of 1.72 eV, followed by Li-b → Li–C → Li-h → Li–H. The values of Δh follow the binding energy opposing trend of Li–H → Li-h → Li–C → Li-b → Li–V_{CH}. The Li–V_{CH} configuration has the shortest Δh suggesting that the Li adatom is more free to approach the three dangling C atoms surrounding the V_{CH} vacancy. This observation is in consensus with the previous results of a Li adatom above a C vacancy in a graphene monolayer.[55,56] To quantify an interaction between Li and the *graphane* system, the amount of charge transfer q was calculated using the Bader charge analysis.[57] Table 2 shows that the sign of the q values is positive, indicating that an amount of charge has been transferred from the foreign atom to the substrate, owing to the low electron affinity of the Li atom (0.62 eV) compared to that of the C atom (1.26 eV). Apart from configuration Li–H with 0.19e, all other configurations possess an average of 0.9e charge transfer.

Since our results revealed that a Li–V_{CH} configuration gives a stable structure, and that the Li atom bonds strongly with the *graphane* substrate although ionically, we further examined its charge density distribution. Fig. 5(a) and (c) show the iso-surfaces of difference charge density ($\Delta\rho$) of the V_{CH} vacancy in a *graphane* monolayer and the Li atom on the V_{CH} vacancy in a *graphane* monolayer, respectively. $\Delta\rho$ is calculated as the difference between the initial atomic charge density used to start the calculation and the final converged charge density. The red iso-surfaces in Fig. 5 indicate where the electrons would prefer to go during the electronic cycles. Fig. 5(b) is the side view of charge density distribution of the V_{CH} vacancy to show clearly that no charge is accumulated on the C atom but is on the H atom. Fig. 5(a) shows that the charge density distribution of the V_{CH} vacancy in a *graphane* monolayer is non-uniform, it is mainly localized around the H atoms as well as at the C–C bond center. Since the C–C bonding in a *graphane* monolayer is covalent, $\Delta\rho$ indicates that the electronic charge densities are minimal at the C atoms (depletion region) but increase towards the center of C–C bonds (accumulation region). We suggest the charge density global minimum region to be at the V_{CH} vacancy. Fig. 5(c) shows that the charge density distribution of the Li–V_{CH} configuration is also non-uniform. It is noted in Fig. 5(c) that there are no charge densities accumulated around the Li atom and C–Li bonds. It has been established earlier in this study that Li donates most of its electronic charge ionically to its three nearest neighbour C atoms, and gains the positive charge which can be interpreted as a depleted region. Hussain *et al.*[35] reported that in a pristine *graphane* monolayer, most of the Li charge is transferred to six C atoms to which the Li atom is covalently bonded. Fig. 5(c) shows that there is no iso-surface charge density on the three C atoms bonded to the Li atom, but that the charge density is slightly enhanced along the C–C bonds closest to the Li adatom as compared to the other C–C bonds far away. This suggests that the three C atoms bonded to the Li atom can also be regarded as depleted regions because the charge density accumulated from the Li adatom has been further shared with their nearest neighbour C atoms as interpreted from the $\Delta\rho$ plot (Fig. 5(c)).

We further studied the response of the Li–V_{CH} structure on the Li charge state alteration. The effect of Li nominal charge doping $q = -1$, 0 and +1 on the thermodynamic stability and structural and electronic properties of the Li–V_{CH} structure (denoted as Li^{1-}–V_{CH}, Li^{0}–V_{CH} and Li^{1+}–V_{CH}) was examined. To study the thermodynamic stability, the formation energy E_f^q(Li–V_{CH}) and charge transition levels $\varepsilon(q/q')$ are calculated using eqn (2) and (4) respectively.

The formation energies for the Li–V_{CH} configuration in its various nominal charge states Li^{1-}–V_{CH}, Li^{0}–V_{CH} and Li^{1+}–V_{CH} as a function of E_F are shown in Fig. 6. Calculated at $E_F = 0$ eV, the formation energy for Li^{0}–V_{CH} is 2.42 eV, lower than that of V_{CH}^{0} by the magnitude of 3.46 eV, revealing an enhancement of the V_{CH}^{0} vacancy stability by the Li atom. Furthermore, Fig. 6 shows that the formation energy for Li^{1+}–V_{CH} is the lowest for the entire bottom half of the band gap up to $E_F = 2.70$ eV, indicating that Li–V_{CH} may likely act as a deep donor. At the VBM ($E_F = 0$ eV), its formation energy is negative (−0.25 eV) revealing the spontaneous (exothermic) formation of the Li ion (Li^{+}) in the V_{CH} vacancy system. In the Li^{1+}–V_{CH} configuration, the Li adatom relaxes to a Δh of 1.51 Å from 1.54 Å for Li^{0}–V_{CH}. The lowest formation energy and small Δh suggest that creation of an ion in a Li–V_{CH} configuration further enhances the binding force between a Li atom and the three dangling C atoms adjacent to the V_{CH} vacancy. On the other hand, the formation energy for the Li^{1-}–V_{CH} configuration is 6.49 eV at $E_F = 0$ eV. This value decreases as the value of E_F increases across the band gap and becomes most stable from $E_F = 4.00$ eV to the CBM. The Li adatom relaxes to a Δh of 1.86 Å above the V_{CH} revealing a relatively weak binding.

The charge transition energy levels for the Li–V_{CH} configurations obtained from eqn (4) are represented by the intersection of the formation energy lines on the *graphane* band gap shown in Fig. 6. The charge transition energy level values are $\varepsilon(0/+1) = 2.70$ eV relative to the VBM (1.75 eV from the CBM) and $\varepsilon(0/-1) = 3.98$ eV (0.47 eV below the CBM). Comparing Fig. 6 and 2(b), it is noted that the effect of Li is to slightly shift both the donor and acceptor charge transition levels of V_{CH} towards the CBM. Nonetheless, the Li–V_{CH} configuration acts as a deep donor, and does not induce n-type conductivity in the *graphane* monolayer.

To gain an insight into the electronic properties of the Li–V_{CH} configuration, the TDOS were computed and plotted in Fig. 7. Fig. 7(a)–(c) depict the TDOS for Li^{1-}–V_{CH}, Li^{0}–V_{CH} and Li^{+}–V_{CH} respectively. Firstly, we compared the TDOS for the V_{CH}^{0} defect depicted in Fig. 4(b) with those of Li^{0}–V_{CH} as shown in Fig. 7(b). The Li introduces the fully occupied states at 0.85 eV above the VBM in the spin-down channel. The V_{CH}^{0} system is half-metallic ferromagnetic (see Fig. 4(b)), but for the Li^{0}–V_{CH} system, the Li atom fills up the V_{CH} partially occupied C 2p states slightly pushing the E_F upwards. The fully occupied induced states, only in the majority spin, are noted at the vicinity of the E_F. Consequently, the Li^{0}–V_{CH} system is ferromagnetic with an integral magnetic moment of 2.00 μ_B per supercell, more than that of V_{CH}^{0} by 1.00 μ_B. We further

examined the origin of the magnetism in a Li^0–V_{CH} system using the PDOS shown in Fig. 7(d). The pronounced C 2p states and small contributions of the C 2s states hybridize with the Li 2s states at the vicinity of the E_F. Typically, enhancement of the magnetic moment by 1.00 μ_B should be due to the influence of the Li valence electron and its orbital occupancy (C 2p orbital states) on the C atoms.

For the Li^{1-}–V_{CH} configuration, the effect of −1 charge doping is to shift the E_F towards the CBM, leaving most of the induced in gap states occupied as shown in Fig. 7(a). As a result, an integral magnetic moment of 3.00 μ_B per supercell is attainable. An enhancement of the magnetism in a Li^{1-}–V_{CH} configuration indicates that an injected electron does localize on the defects and is not distributed all over the supercell space. The Li^{1-}–V_{CH} configuration is half-metallic ferromagnetic as revealed by the TDOS plot shown in Fig. 7(a), and also possesses the features of an n-type donor system. For the Li^{+}–V_{CH} configuration, creation of the Li ion shifts the E_F as well as the corresponding occupied majority spin states by 1.10 eV towards the VBM as shown in Fig. 7(c), revealing the feature of a deep donor system. The effects of +1 charge doping remove the Li induced occupied spin-down states at 0.85 eV above the VBM. As a result, the induced magnetic moment becomes 1.00 μ_B per supercell. This deviation in magnetism suggests that an ejected electron should originate from the Li 2s orbital states. An understanding of the variation of the induced magnetism due to charge state alteration should be clear when considering an idea of the simple electronic counting from the DOS analysis. It is concluded that V_{CH} defect magnetism can be evolved due to the influence of the Li adsorption as well as its charge state alteration.

Conclusions

We used a hybrid DFT approach (HSE06) to study the interaction of a Li atom with a V_{CH} vacancy defect in a *graphane* monolayer. Firstly, the effects of a V_{CH} defect in a *graphane* monolayer were investigated in terms of the stability and structural, magnetic and electronic properties, involving the influence of charge doping. The formation energies plot analysis revealed that only the −1, 0 and +1 charge states are thermodynamically stable within the *graphane* band gap, and that the V_{CH} vacancy is a single deep donor defect, and may likely compensate the acceptor depending on the position of E_F. The local geometry of a V_{CH} defect is very sensitive to the charge doping. Our results suggest that a V_{CH} defect induces half-metallic stable ferromagnetism in a *graphane* monolayer mainly originating from the C 2p orbital states. The −1 (+1) charge doping doubles (suppresses) the V_{CH} defect induced magnetic moment, and yields a spin polarized n-type (non-spin polarized) system. In conclusion, the electronic structure of a V_{CH} defect in the *graphane* monolayer can be controlled *via* charge state modulation.

Secondly, a Li adatom was introduced into a V_{CH} defect in the *graphane* system and also charged. It was found that the Li enhances the thermodynamic stability of a V_{CH} defect. The formation energy as a function of E_F plot indicates that the Li–V_{CH} system may likely act as a single deep donor, and is ready to compensate the acceptor. The Li introduces more occupied states in the band gap, and also there is hybridization between the C 2p states and Li 2s states at the vicinity of the E_F in the spin-up channel only, leading to enhancement of the magnetism. The −1 charge doping (Li^{1-}–V_{CH}) further populates the occupied states in the band gap shifting the E_F towards the CBM. Consequently, the Li^{1-}–V_{CH} system is half-metallic ferromagnetic, and possesses pronounced magnetism. The +1 charge doping (Li^{1+}–V_{CH}) removes some of the Li induced occupied states, slightly shifting the E_F towards the VBM leading to a reduction in the magnetic moment. An understanding of the variation of the induced magnetism due to charge state alteration should be clear when considering an idea of the simple electronic counting from the density of states analysis. Our findings give an explanation of the origin of magnetism in a V_{CH} defective *graphane* system and suggest a possible practical way of controlling it.

Acknowledgements

The authors would like to thank the University of Pretoria, University of South Africa and the National Research Foundation (NRF) for support. We are grateful to Prof. J. Pretorius and Prof. W. Meyer for assisting with the VASP code. REM is grateful to Mr E. Igumbor for fruitful discussions. NC thanks the National Institute for Theoretical Physics (NIThep) for financial support.

References

1 J. O. Sofo, A. S. Chaudhari and G. D. Barber, *Phys. Rev. B: Condens. Matter Mater. Phys.*, 2007, **75**, 153401.
2 D. C. Elias, R. R. Nair, T. M. G. Mohiuddin, S. V. Morozov, P. Blake, M. P. Halsall, A. C. Ferrari, D. W. Boukhvalov, M. I. Katsnelson, A. K. Geim and K. S. Novoselov, *Science*, 2009, **323**, 610.
3 A. Savchenko, *Science*, 2009, **323**, 589.
4 K. S. Novoselov, A. K. Geim, S. V. Morozov, D. Jungian, Y. Zhang, S. V. Dubonos, I. V. Grigorieva and A. A. Firsov, *Science*, 2004, **306**, 666.
5 A. K. Geim and K. S. Novoselov, *Nat. Mater.*, 2007, **6**, 183.
6 P. R. Wallace, *Phys. Rev.*, 1947, **71**, 622.
7 K. S. Novoselov, A. K. Geim, S. V. Morozov, D. Jiang, Y. Zhang, M. I. Katsnelson, S. V. Dubonos, I. V. Grigorieva and A. A. Firsov, *Nature*, 2005, **438**, 197.
8 K. S. Novoselov, Z. Jiang, Y. Zhang, S. V. Morozov, H. L. Stormer, U. Zeitler, J. C. Maan, G. S. Boebinger, P. Kim and A. K. Geim, *Science*, 2007, **315**, 1379.
9 O. Leenaerts, H. Peelaers, A. D. Hernandez-Nieves, B. Partoens and F. M. Peeters, *Phys. Rev. B: Condens. Matter Mater. Phys.*, 2010, **82**, 195436.
10 D. W. Boukhvalov, M. I. Katsnelson and A. I. Lichtenstein, *Phys. Rev. B: Condens. Matter Mater. Phys.*, 2008, **77**, 035427.
11 D. W. Boukhvalov and M. I. Katsnelson, *Phys. Rev. B: Condens. Matter Mater. Phys.*, 2008, **78**, 085413.

12 F. Karlicky, R. Zboril and M. Otyepka, *J. Chem. Phys.*, 2012, **137**, 034709.
13 A. Z. Alzahrani and G. P. Srivastava, *Appl. Surf. Sci.*, 2010, **256**, 5783.
14 H. Sahin, O. Leenaerts, S. K. Singh and F. M. Peeters, *WIREs. Comput. Mol. Sci.*, 2015, **5**, 255.
15 S. Lebegue, M. Klintenberg, O. Eriksson and M. I. Katsnelson, *Phys. Rev. B: Condens. Matter Mater. Phys.*, 2009, **79**, 245117.
16 P. Chandrachud, B. S. Pujari, S. Haldar, B. Sanyal and D. G. Kanhere, *J. Phys.: Condens. Matter*, 2010, **22**, 465502.
17 H. Sahin, C. Ataca and S. Ciraci, *Appl. Phys. Lett.*, 2009, **95**, 222510.
18 H. Sahin, C. Ataca and S. Ciraci, *Phys. Rev. B: Condens. Matter Mater. Phys.*, 2010, **81**, 205417.
19 C.-K. Yang, *Carbon*, 2010, **48**, 3901.
20 B. Wu and C. Yang, *Appl. Phys. Lett.*, 2012, **2**, 012173.
21 J. Berashevich and T. Chakraborty, *Nanotechnology*, 2010, **21**, 355201.
22 R. E. Mapasha, M. P. Molepo and N. Chetty, *Phys. E*, 2016, **79**, 52–58.
23 A. Y. S. Eng, H. L. Poh, F. Sanek, M. Marysko, S. Matejkova, Z. Sofer and M. Pumera, *ACS Nano*, 2013, **7**, 5930–5939.
24 B. S. Pujari and D. G. Kanhere, *J. Phys. Chem. C*, 2009, **113**, 21063–21067.
25 V. M. Pereira, J. M. B. L. dos Santos and A. H. C. Neto, *Phys. Rev. B: Condens. Matter Mater. Phys.*, 2008, **77**, 115109.
26 A. Zobelli, V. Ivanovskaya, P. Wagner, I. Suarez-Martinez, A. Yaya and C. P. Ewels, *Phys. Status Solidi B*, 2012, **249**, 1521–3951.
27 K. T. Chan, J. B. Neaton and M. L. Cohen, *Phys. Rev. B: Condens. Matter Mater. Phys.*, 2008, **77**, 235430.
28 M. Farjam and R. Tabar, *Phys. Rev. B: Condens. Matter Mater. Phys.*, 2009, **79**, 045417.
29 M. Khantha, N. A. Cordero, L. M. Molina, J. A. Alonso and L. A. Girifalco, *Phys. Rev. B: Condens. Matter Mater. Phys.*, 2004, **70**, 125422.
30 P. A. Denis, *Chem. Phys. Lett.*, 2010, **492**, 251–257.
31 C.-K. Yang, *Appl. Phys. Lett.*, 2009, **94**, 163115.
32 R. E. Mapasha and N. Chetty, *Comput. Mater. Sci.*, 2010, **49**, 787.
33 M. Khazaei, M. S. Bahramy, N. S. Venkataramanan, H. Mizuseki and Y. Kawazoe, *J. Appl. Phys.*, 2009, **106**, 094303.
34 T. Hussain, B. Pathak, T. A. Maark, C. M. Araujo, R. H. Scheicher and R. Ahuja, *EPL*, 2011, **96**, 27013.
35 T. Hussain, B. Pathak, T. A. Maark, R. Ramzan and R. Ahuja, *EPL*, 2012, **99**, 47004.
36 T. Hussain, B. Pathak, A. D. Sarkar and R. Ahuja, *Appl. Phys. Lett.*, 2012, **101**, 103907.
37 S. Watcharinyanon, L. I. Johansson, A. A. Zakharov and C. Virojanadara, *Surf. Sci.*, 2012, **606**, 3.
38 C. G. Van de Walle and J. Neugebauer, *J. Appl. Phys.*, 2004, **95**, 3851.
39 J. Heyd, G. E. Scuseria and M. Ernzerhof, *J. Chem. Phys.*, 2003, **118**, 8207.
40 J. Heyd and G. E. Scuseria, *J. Chem. Phys.*, 2004, **121**, 1187–1192.
41 A. Janotti and C. G. Van de Walle, *Phys. Status Solidi B*, 2011, **248**, 799.
42 H.-P. Komsa and A. Pasquarello, *Phys. Rev. B: Condens. Matter Mater. Phys.*, 2011, **84**, 075207.
43 G. Kresse and J. Hafner, *Phys. Rev. B: Condens. Matter Mater. Phys.*, 1993, **47**, 558.
44 G. Kresse and J. Hafner, *Phys. Rev. B: Condens. Matter Mater. Phys.*, 1994, **49**, 14251.
45 G. Kresse and J. Furthmuller, *Phys. Rev. B: Condens. Matter Mater. Phys.*, 1996, **54**, 11169.
46 G. Kresse and J. Furthmuller, *Comput. Mater. Sci.*, 1996, **6**, 11169.
47 P. E. Blochl, *Phys. Rev. B: Condens. Matter Mater. Phys.*, 1994, **50**, 17953.
48 H. J. Monkhorst and J. D. Pack, *Phys. Rev. B: Condens. Matter Mater. Phys.*, 1976, **13**, 5188.
49 M. Methfessel and A. T. Paxton, *Phys. Rev. B: Condens. Matter Mater. Phys.*, 1989, **40**, 3616.
50 G. Makov and M. C. Payne, *Phys. Rev. B: Condens. Matter Mater. Phys.*, 1995, **51**, 4014.
51 J. P. Perdew, K. Burke and M. Ernzerhof, *Phys. Rev. Lett.*, 1996, **77**, 3865.
52 J. Q. Hu, J. H. Zhang, S. Q. Wu and Z. Z. Zhu, *Solid State Commun.*, 2015, **209**, 210.
53 M. N. Amini, O. Leenaerts, B. Partoens and D. Lamoen, *J. Phys. Chem. C*, 2013, **117**, 16242–16247.
54 R. C. Andrew, R. E. Mapasha and N. Chetty, *J. Chem. Phys.*, 2013, **138**, 244709.
55 K. M. Fair, X. Y. Cui, L. Li, C. C. Shieh, R. K. Zheng, Z. W. Liu, *et al.*, *Phys. Rev. B: Condens. Matter Mater. Phys.*, 2013, **87**, 014102.
56 S. Seenithurai, R. K. Pandyan, S. V. Kumar, C. Saranya and M. Mahendran, *Int. J. Hydrogen Energy*, 2014, **39**, 11016–11026.
57 R. F. W. Bader, *Atoms in Molecules-A Quantum Theory*, Oxford University Press, Oxford, 1990.